Fully Implantable Neurostimulation System for Long-Term Behavioral Animal Study

Wonok Kang, Jinseung Lee, Wonsuk Choi, Jinseok Kim, Junesun Kim, and Sung-Min Park, *Senior Member, IEEE*

***Abstract*— Spinal cord stimulation (SCS) is an emerging therapeutic option for patients with neuropathic pain due to spinal cord injury (SCI). Numerous studies on pain relief effects with SCS have been conducted and demonstrated promising results while the mechanisms of analgesic effect during SCS remain unclear. However, an experimental system that enables large-scale long-term animal studies is still an unmet need for those mechanistic studies. This study proposed a fully wireless neurostimulation system that can efficiently support a long-term animal study for neuropathic pain relief. The developed system consists of an implantable stimulator, an animal cage with an external charging coil, and a wireless communication interface. The proposed device has the feature of remotely controlling stimulation parameters via radio-frequency (RF) communication and wirelessly charging via magnetic induction in freely moving rats. Users can program stimulation parameters such as pulse width, intensity, and duration through an interface on a computer. The stimulator was packaged with biocompatible epoxy to ensure long-term durability under *in vivo* conditions. Animal experiments using SCI rats were conducted to demonstrate the functionality of the device, including long-term usability and therapeutic effects. The developed system can be tailored to individual user needs with commercially available components, thus providing a cost-effective solution for large-scale long-term animal studies on neuropathic pain relief.**

***Index Terms*— Spinal cord stimulation (SCS), spinal cord injury (SCI), pain relief, implantable stimulator, survival study.**

Manuscript received 14 February 2023; revised 22 June 2023 and 20 August 2023; accepted 10 September 2023. Date of publication 14 September 2023; date of current version 22 September 2023. This work was supported in part by the Pioneer Research Center Program through the National Research Foundation of Korea (NRF) funded by the Ministry of Science and Information and Communication Technology (ICT) under Grant 2022M3C1A3081294; in part by the National Research and Development Program through NRF funded by the Ministry of Science and ICT under Grant 2021M3H4A1A03049084; in part by the Basic Science Research Program through NRF funded by the Ministry of Education under Grant 2020R1A6A1A03047902; in part by the Basic Science Research Program through NRF funded by the Ministry of Science and ICT under Grant NRF-2017R1A5A1015596; and in part by the 2021 Joint Research Project of Institutes of Science and Technology. *(Wonok Kang and Jinseung Lee contributed equally to this work.) (Corresponding authors: Junesun Kim; Sung-Min Park.)*

This work involved animals in its research. Approval of all ethical and experimental procedures and protocols was granted by the Korea University Institutional Animal Care and Use Committee under Approval No. KUIACUC-2021-0103.

Wonok Kang is with the Department of Convergence IT Engineering and the Medical Device Innovation Center, Pohang University of Science and Technology, Pohang 37673, South Korea (e-mail: wonokkang@postech.ac.kr).

Jinseung Lee is with the Rehabilitation Science Program, Department of Health Science, and the Transdisciplinary Major in Learning Health Systems, Department of Healthcare Science, Graduate School, Korea University, Seoul 02841, South Korea.

Wonsuk Choi is with the Center for Bionics, Korea Institute of Science and Technology, Seoul 02792, South Korea, and also with the School of Biomedical Engineering, Korea University, Seoul 02841, South Korea.

Jinseok Kim is with the Center for Bionics, Korea Institute of Science and Technology, Seoul 02792, South Korea.

Junesun Kim is with the Rehabilitation Science Program, Department of Health Science, the Transdisciplinary Major in Learning Health Systems, Department of Healthcare Science, Graduate School, and the Department of Health and Environmental Science, Undergraduate School, Korea University, Seoul 02841, South Korea (e-mail: junokim@korea.ac.kr).

Sung-Min Park is with the Department of Convergence IT Engineering, the Department of Electrical Engineering, the Department of Mechanical Engineering, and the Medical Device Innovation Center, Pohang University of Science and Technology, Pohang 37673, South Korea (e-mail: sungminpark@postech.ac.kr).

Digital Object Identifier 10.1109/TNSRE.2023.3315371

I. Introduction

NEUROPATHIC pain due to nerve damage or injury affects approximately 8% of the general population [1], [2]. Analgesic medication is the first therapeutic option for patients with neuropathic pain; however, only half of the patients experience partial relief with this pharmacological approach [3]. Neuromodulation methods, including deep brain stimulation, peripheral nerve stimulation, non-invasive magnetic stimulation, and spinal cord stimulation (SCS), have emerged as alternative therapeutic options for patients not eligible for pharmacological treatment [4]. Among these stimulation modalities, SCS, the only available device-based therapy in the current clinical setting, has attracted particular interest as a promising technique due to its precise pain control capability. SCS therapy induces a neuromodulatory effect that controls pain perception by delivering small amounts of electrical stimulus energy to spinal structures, mostly in the dorsal column [5]. The pain relief effects of SCS have been clinically validated extensively; however, the underlying mechanisms of the analgesic effects of various stimulation modalities have yet to be fully elucidated, and thus studies for uncovering them are continually being conducted.

For several decades, numerous studies on pain relief have been conducted using conventional tonic stimulation

(delivering low frequencies of <100 Hz), high-frequency stimulation (500–10000 Hz), and burst stimulation (delivering pulse trains of hundreds of Hz) waveforms [6]. Conventional tonic SCS therapy has been primarily used in animal studies and clinical trials and has also been applied in clinical practice (Intellis™Rechargeable SCS, Medtronic, USA); however, the process may involve suboptimal pain relief and paresthesia, making patients indisposed [7]. High-frequency and burst SCS demonstrated substantial improvement in pain treatment while preventing paresthesia due to the subthreshold stimulation of the Aβ fibers, providing patients with alternative therapeutic options [8], [9], [10]. With the promising results, these stimulation modalities have been considered the ultimate neuromodulation solution for neuropathic pain; however, it is still premature to fully take these modalities as a standard treatment because high-frequency control sacrifices some practical benefits of conventional tonic SCS. In particular, high-frequency stimulations consume more energy than low-frequency stimulations, limiting the lifetime of devices and requiring frequent battery changes. In addition, a slow response to therapeutic effects makes it difficult to optimize and evaluate the stimulation parameters in a single session [11].

Efforts to find a new stimulation modality that overcomes the above-mentioned limitations are still ongoing through animal experiments. Conventional SCS systems used in animal studies typically comprise a thin electrode array, external stimulus generator, and rotating connector [12], [13]. The electrode array is placed in the epidural space and connected to the stimulus generator via a rotating connector, preventing the twisting and over-tensioning of the cable. Occasionally, a transcutaneous button that freely allows attachment and detachment of the cable is installed on the head or back of the rats. However, this conventional method with external devices is more likely to induce local wound infections and transmit them to the epidural space compared with a fully implantable system that limits the test duration to a maximum of 7–14 days [14]. This limited experimental time makes it impossible to conduct long-term evaluations, which are needed to comprehensively investigate the therapeutic effects of various stimulation conditions and determine optimal parameters, such as frequency, intensity, and pulse shape. Furthermore, conventional wired systems make behavioral and biological investigations more labor-intensive because they require researchers to be physically present to perform experiments on a limited number of animals at a time [15]. These limitations often result in human-induced errors; thus, the reproducibility of experimental results may become questionable.

In this regard, fully implantable neuromodulators have been proposed in recent years to investigate various diseases, such as epilepsy, overactive bladder, essential tremor, diabetes, and chronic pain [16], [17]. Wireless and fully implantable neurostimulation techniques, which can be used in freely moving rodents, have been proposed due to the high translational relevance of an awake model [16]. In addition, a scalable and modular wireless network infrastructure with an implantable optical stimulator was proposed for large-scale behavioral studies [15]. In this context, developing experimental systems for large-scale and long-term animal experiments using inexpensive commercial components can accelerate many scientific findings.

TABLE I
REQUIREMENTS FOR SYSTEM DESIGN

	Requirement
Power	24/7 Rechargeable without anesthesia or restrain
Packaging	Over 3 months with biocompatibility
Stim amplitude	Over 1 mA with several μA step
Stim frequency	Conventional tonic, high-frequency, and burst SCS
Control	Wireless communication with user interface
Size	Implantable on the back of rodents

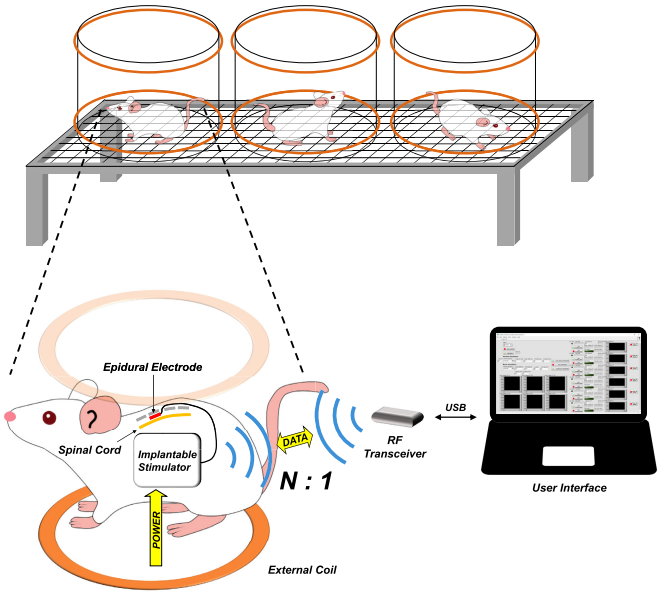

Fig. 1. Conceptual illustration of the proposed experimental system.

In this study, we developed a fully implantable neurostimulation system for long-term behavioral and biological investigations of neuropathic pain relief using commercially available components. Subsequently, *in vitro* and *in vivo* experiments were performed to evaluate the performance and functionality of the proposed device. The remainder of this paper is organized as follows: Section II presents the detailed implementation, including the system architecture, functional blocks, and design parameters; Sections III and IV describe the preparation and results of the *in vitro* and *in vivo* experiments, respectively; Section V includes a comprehensive discussion of the proposed device; and Section VI concludes the paper.

II. System Implementation

Design requirements were considered prior to developing the proposed implantable SCS system for neuropathic pain relief research. 1) Device longevity related to the battery run time and the device packaging durability is important for comprehensive and long-term evaluation of therapeutic effects for various conditions. 2) Controllable stimulus parameters with a wide range of frequencies, pulse widths, and amplitudes should be provided to the user. 3) Implantable device should have a proper volume that does not affect the normal

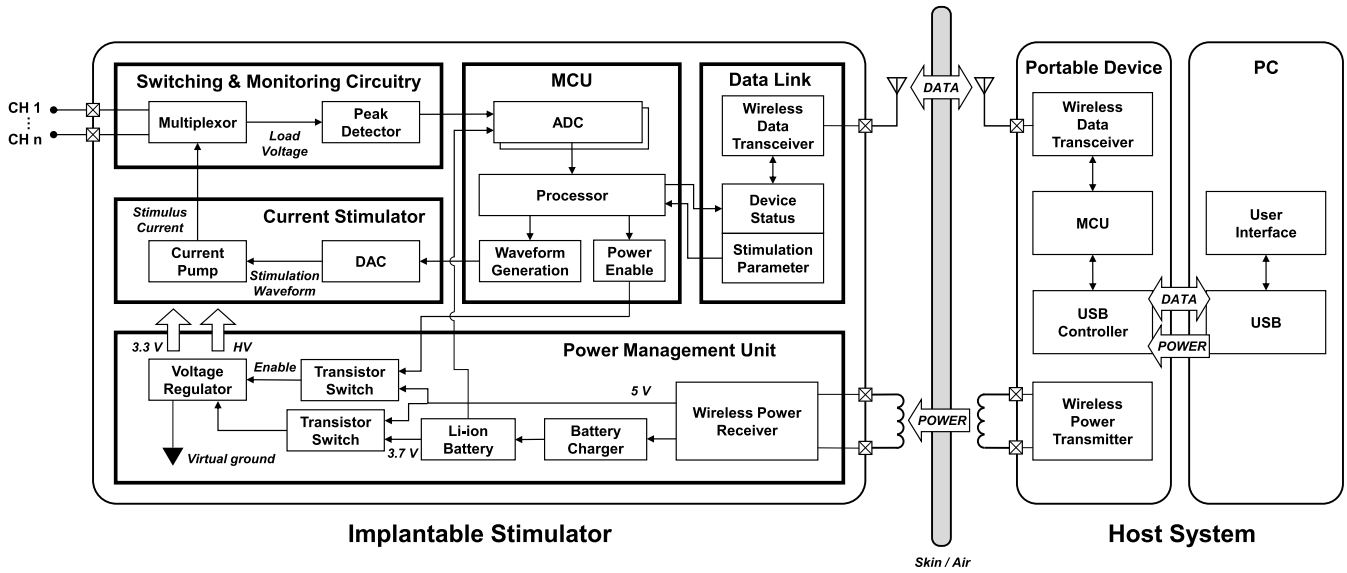

Fig. 2. System block diagram.

motor function of animals under testing. 4) Multi-device control using wireless communication is required for simultaneous multi-subject experiments. Overall system requirements including the above considerations are summarized in Table I.

A. System Overview

Figure 1 shows the overall experimental setup for behavioral investigation in multiple rats using the proposed implantable device. An epidural electrode for spinal cord stimulation was implanted in the epidural space and wired with an implantable stimulator. The implant receives power from an external charging coil surrounding the individual cage and communicates wirelessly with the user via a radio-frequency (RF) transceiver. In addition, the user can simultaneously control several devices implanted in multiple rats through a single user interface.

Figure 2 shows a block diagram of the entire system, comprising an implantable stimulator, a portable external device, and a personal computer (PC). The proposed implantable stimulator is composed of five primary building blocks: 1) power management unit (PMU), 2) current stimulation circuitry, 3) stimulation switching and monitoring circuitry, 4) wireless transceiver, and 5) microcontroller unit (MCU). The PMU provides a supply voltage to all circuits either from a battery or wirelessly delivered power. The current source circuit can generate a current stimulus from 10 μA to 2000 μA in steps of 10 μA. The multiplexor selects the direction of the stimulation current and activated channel. The peak detection circuitry measures the load voltage to determine the saturation of the drive voltage. The wireless data transceiver is used to program a stimulation protocol that is commanded by an external host to the implantable stimulator and transmit the device status to the host wirelessly via 2.4 GHz industrial scientific and medical (ISM) bands. The MCU controls the operation of all components, including recording voltage data, processing stimulus parameters, and communication via the RF transceiver. The user can control the implantable device's

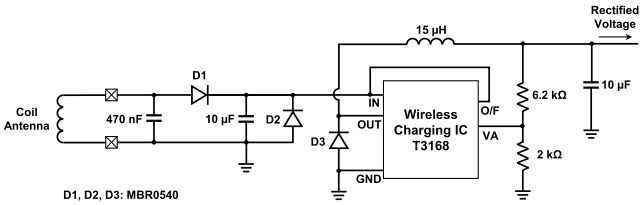

Fig. 3. Wireless power transfer receiving circuit.

wireless power supply and data communication functions using a portable RF transceiver connected to the PC through a graphical user interface (GUI).

B. Power Supply via Rechargeable Battery or Wireless Power Transfer

Embedding a wireless power transfer (WPT) function into the implant is essential to avoid frequent battery replacement surgeries. A transmitting (Tx) coil was constructed by wrapping a cylindrical acrylic cage in a helical manner using 36-AWG/300-strand Litz wire (240 mm diameter, 6 turns; YDK, Korea). A receiving (Rx) coil consisted of a square coil surrounding the stimulator circuit using 34-AWG Teflon insulated wire (38 mm × 38 mm; SME, Korea). The Tx coil was driven by a power amplifier (LPA05, Newtons4th, UK) and signal generator (33220A, Agilent Technologies, USA). Moreover, a power receiving circuit with a wireless charging integrated circuit (IC) (T3168, Taidacent, China) and several passive/active components were adopted, as shown in Figure 3. The Rx circuit generates rectified power when the voltage applied to the Rx coil exceeds a threshold. The maximum current output of receiving circuit was 600 mA for a 5 V supply.

Figure 4 shows that the load-sharing circuitry [18], constructed using a P-channel MOSFET (FDN336P, Onsemi, USA), Schottky diode (NSR0230M2T5G, Onsemi), and

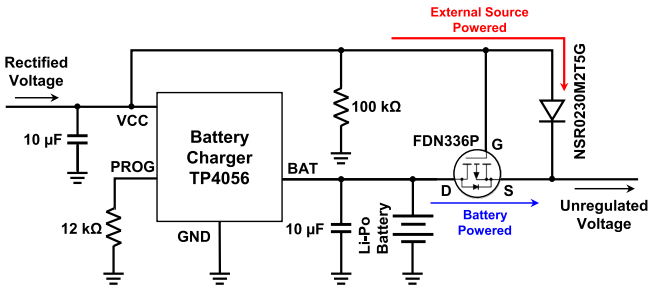

Fig. 4. Power source selector circuit.

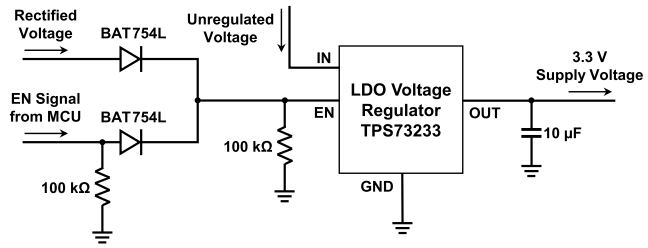

Fig. 5. Low-voltage regulator and digital power switch circuit.

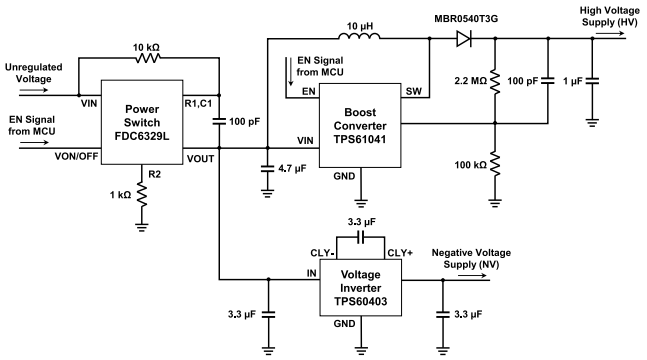

Fig. 6. High-voltage boosting circuit with the values specified on passive components.

TABLE II
PROGRAMMABLE STIMULATION PARAMETERS FOR EACH MODE

Parameters \ Mode	Normal	Burst
Pulse width	24–9999 µs	24–2000 µs
Intensity	10–2000 µA	10–2000 µA
Duration	1–7200 s	1–7200 s
Frequency	1–10000 Hz	71–14706 Hz
Number of pulses	N/A	5–50
Interphase gap	N/A	1–1000 ms

pull-down resistor (100 kΩ), can select the power delivered to other circuits from either the external power supply or battery. The rectified voltage from the WPT Rx circuit can recharge the lithium-polymer (Li-Po; 3.7 V, 170 mAh, Maxpower, China) battery via a battery management IC (TP4056, TPOWER, China).

To maximize the battery life of the proposed device, the shutdown function of the low-dropout (LDO) voltage regulator (TPS73233, Texas Instruments, USA) was utilized (Figure 5). When power is wirelessly delivered to the implant, the enable (EN) pin of the LDO regulator is pulled high, and the LDO regulator generates 3.3 V to power the MCU. Once the MCU receives power, it maintains its power state by pulling the EN pin high until it is commanded to shut down.

C. Electrical Stimulation Circuit With Load Monitor

To provide a stable supply voltage for the current source and switches without saturation even at a high load impedance, a boost converter TPS61041 (TI) was used to convert the supply from the battery or the WPT into a 28 V supply (Figure 6). The MCU controls a load switch (FDC6329L, Onsemi) to eliminate the standby power of the boost converter.

Figure 7 shows a schematic of the current stimulator and load monitor. The voltage waveform was generated by the MCU and a digital-to-analog converter (DAC; 12-bit resolution, MCP4821, Microchip, USA). Subsequently, this waveform was applied to the voltage-controlled current source (VCCS) that converts the constant voltage to a constant current, including during load impedance change conditions [19]. An operational amplifier (OP Amp) AD8684 Analog Devices, USA) was adopted to implement a feedback circuit for the VCCS due to its high speed, low power consumption, and wide bandwidth. Two multiplexers (MAX4535, Maxim Integrated, USA) were used to implement the switching circuitry; one was used to construct the H-bridge structure (determining the direction of the stimulus current for charge-balanced biphasic stimulation) and the other to select the activated channels. In long-term experiments, the implanted electrode may be damaged or corroded due to mechanical mismatch and chemical reactions, resulting in tissue stimulation failure. If the implanted electrode is defective, the output voltage across the load would be saturated (open circuit) or zero (short circuit). Electrode failure can therefore be easily determined by measuring the driven voltage. However, detecting fast waveforms requires high sampling rates and burdensome computations. Thus, a load-monitoring function capable of detecting failures by observing impedance changes at low sampling rates was built using a peak detector and voltage buffer.

Figure 8 and Table II show the designed stimulation patterns and values under the normal and burst modes, which are commonly used SCS parameters for animal and clinical studies. The normal mode provides a wide range of stimulus frequencies, from 1 to 10,000 Hz, covering the frequency of conventional tonic and high-frequency stimulation. The burst mode also offers a wide range of parameter controls for various parametric studies. All types of stimuli were designed with biphasic waveforms using a high-precision source to avoid charge balance problems that can lead to electrode corrosion [20]. The proposed device provides flexibility to researchers by enabling control of various parameters using a GUI.

D. Wireless Communication and Data Processing Unit

An nRF24L01+ RF transceiver module (Nordic Semiconductor, Norway) operating in the 2.4 GHz ISM band and supporting data pipe for simultaneous multiple communication

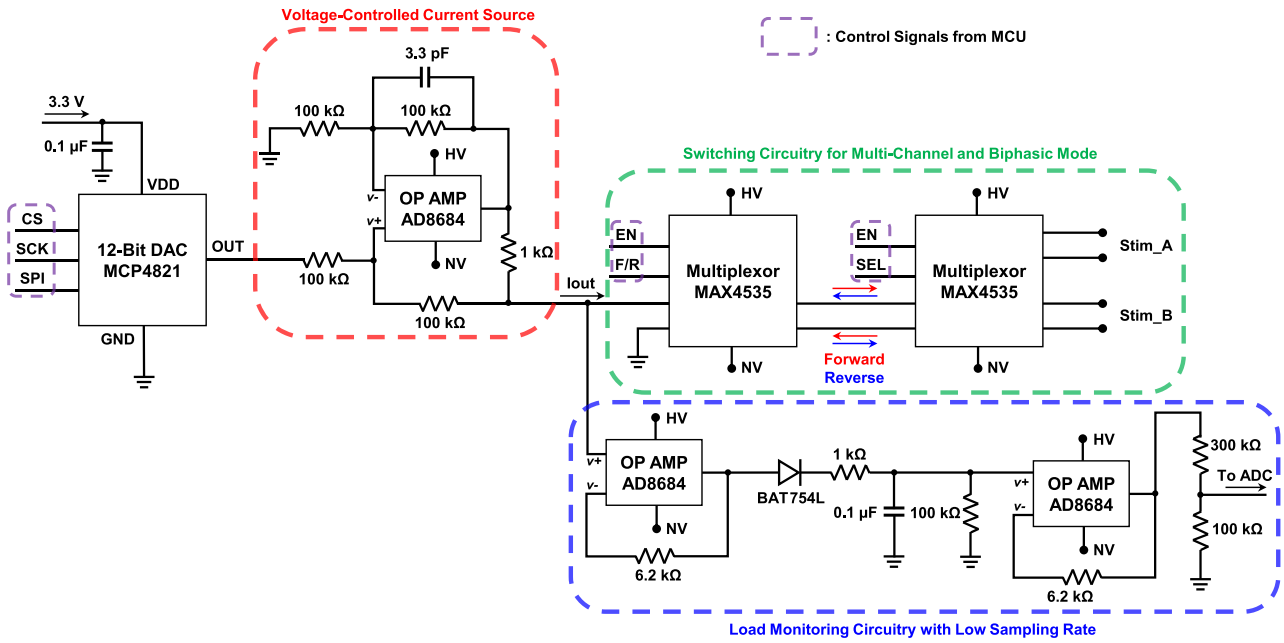

Fig. 7. Biphasic current stimulator and load monitoring circuitry.

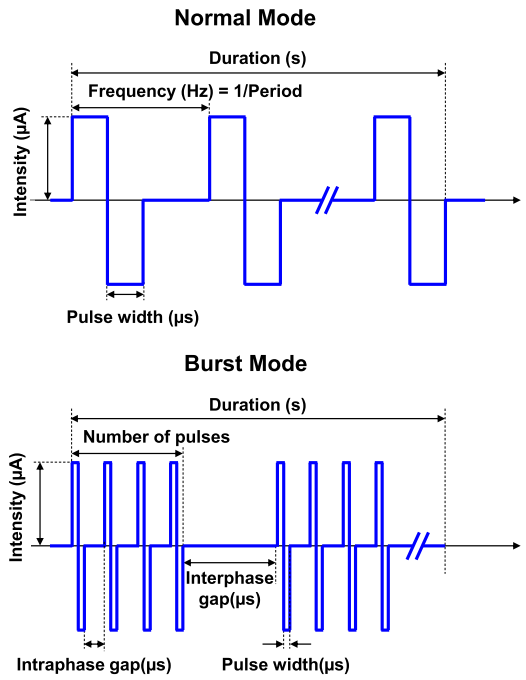

Fig. 8. Stimulation patterns of the proposed SCS device.

was used to deliver the data, including the remaining battery life, stimulation parameters, and device identification number. All data processing and IC instructions were performed using the MCU (ATmega328P, Microchip). The MCU was programmed to periodically enter the power saving mode to minimize standby power consumption.

E. Graphical User Interface

A GUI was developed using a commercial system design platform (LabVIEW 2017, National Instruments, USA) to enhance user convenience related to device manipulation. The user can check information, such as the remaining battery level, load voltage, elapsed time after stimulation, and number of devices transmitted from the implant, through the GUI. In addition, the GUI provides the user with a stimulation command delivery function with various parameters, including stimulus frequency, intensity, pulse width, and total stimulation time.

F. System Integration With Biocompatible Packaging

Figure 9 shows the printed circuit board (PCB) and implantable stimulation system. The epidural electrode was designed and manufactured using a microelectromechanical systems (MEMS) technique [21], [22]. Table III presents the specifications including materials, thickness, and dimensions of the electrode. The electrode was connected to a flexible flat cable (FFC) connector mounted on a small PCB and wired to the switching circuitry in the implantable device. Ensuring the durability of the device packaging with biocompatibility for long-term *in vivo* experiments is necessary because body fluids and blood can corrode or damage the electronic and mechanical components embedded in an implantable device. The proposed device was covered with biocompatible epoxy (EPO-TEK 301, Epoxy Technology, USA), widely used in the field of implantable medical devices due to its cost-effectiveness and ease of use [23]. The final dimensions of the integrated device were 40.5 mm × 40.5 mm × 12.5 mm.

III. Benchtop Measurement Results

A. Current Stimulator and Load Voltage Monitor

An *in vitro* experimental setup was built using a saline phantom (Figure 10, (a)) to evaluate the performance of the constant-current stimulator. A 100 Ω resistor was connected

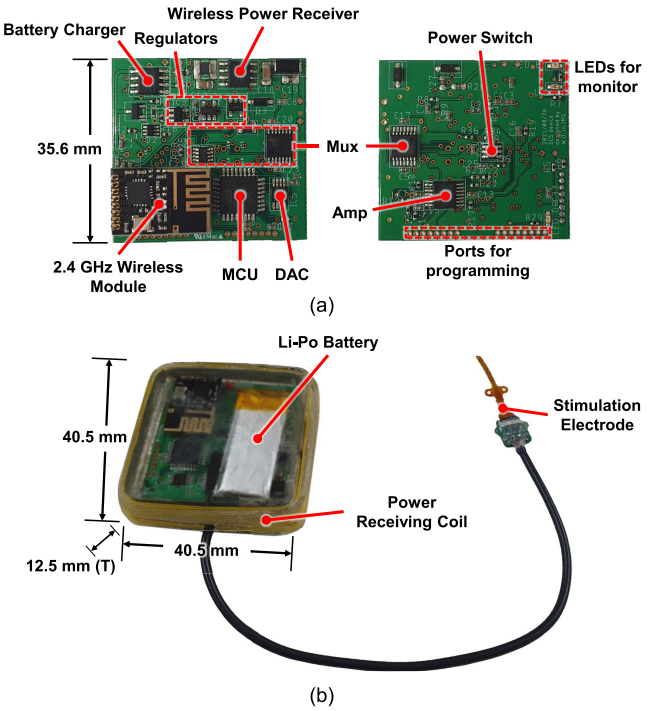

Fig. 9. (a) Fabricated circuit board and (b) fully integrated device after implantable packaging.

TABLE III
SPECIFICATION OF THE EPIDURAL ELECTRODE

Type	One-way row shape
Electrode material	Gold and Polyimide
Array thickness	70 μm
Electrode dimensions	1.1 mm × 0.4 mm
Center-to-center distance	3.0 mm
Number of channels	4

in series with an electrode submerged in the phantom and parallel with a differential amplifier for current measurements. In addition, the load voltage was measured using a peak detector embedded in the device and transferred to the user to check the voltage saturation in the load. Figure 10, (b) and (c) present the measured current waveforms across the shunt resistor (top and middle) and measured load voltage at the current source output (bottom) under conventional and burst stimulations, respectively. The output performance of the stimulator was further investigated with varying stimulation frequency, pulse width, and amplitude (Figure 10, (d); two-way repeated measures ANOVA; $P = 0.098$ and 0.887 for pulse width and amplitude comparisons, respectively; $n = 5$). Figure 11 presents the representative results of the load-monitoring function of the system with normal and defective electrodes. In the normal condition, the load voltage was driven to approximately 10 V, which is within the normal voltage range. However, if the current path in the electrode was shorted or open, the load voltage was measured as 0 V or saturated at the maximum supply voltage.

B. Wireless Charging Performance

The maximum induced current during wireless charging was measured with varying angles between Rx and Tx coils by rotating the orientation of the implantable device. The maximum load current at each tilt angle was determined under the condition of maintaining supply voltage (5 V) stable. It was confirmed that power was delivered stably from 0 to 45°, and power transfer was possible even in bad conditions (60 and 75°). Figure 12 shows the experimental configuration and results in detail.

C. Accelerated Aging Test

The durability of implantable devices is very important for long-term animal experiments. To estimate the expected longevity of the proposed device, an accelerated aging test was conducted in saline phantom (pH 7.4) at 60 °C, giving an approximate acceleration factor of 4.92 [24]. The output current (100 Hz, 200 μs, 200 μA) was stably maintained for 35 days, thus estimated to be equivalent to 180 days at 37 °C (Figure 13).

IV. In Vivo Results

Animal experiments were performed using a rodent model of spinal cord injury (SCI) to demonstrate the functionality of the proposed implantable stimulator for long-term *in vivo* experiments. The devices were implanted into the backs of the rats. Subsequently, the motor threshold (MT) measurement and von Frey test were performed for approximately 1 week and 2 weeks, respectively. In addition, a histological examination was conducted to determine possible structural alternation and tissue damage due to implantation. The methods and results are discussed in the subsequent subsections.

A. Animal Preparation

All animal experiments were approved by the Korea University Institutional Animal Care and Use Committee (KUIACUC-2021-0103). A total of 5 adult male Sprague–Dawley rats (200–220 g, Orient Bio Inc., Seoul, Korea) were used in the experiments. All devices were sterilized with EO gas prior to implantation.

During the entire experimental period including pre-SCI, post-SCI, and post-implantation, joint movement, locomotion, and walking stability were assessed with the Basso, Beattie, and Bresnahan locomotor rating scale (BBB) to determine the effect of device implantation on the rodent's physical conditions [25]. To investigate the analgesic effect of SCS using the proposed stimulator, a contusive SCI was induced at the eleventh thoracic vertebra level (T11) with a 150 kdyn force using the Infinite Horizon Impactor (Precision Systems & Instrumentation, USA) under deep anesthesia (2% isoflurane in O_2) [26]. Subsequently, postoperative treatments, including saline (2.0 ml, subcutaneous) injection for rehydration and manual expression of the bladder, were performed twice a day until spontaneous urination recovered. To prevent urinary tract infection, lactocillin (sulbactam sodium/ampicillin sodium, 100 mg/kg, Aprogen Inc., Korea) was injected intraperitoneally once a day. The stimulation system was implanted 2 weeks after the SCI, when the rats recovered their motor functions and were able to respond to the stimuli. A small laminectomy was performed at L1, and the electrode was

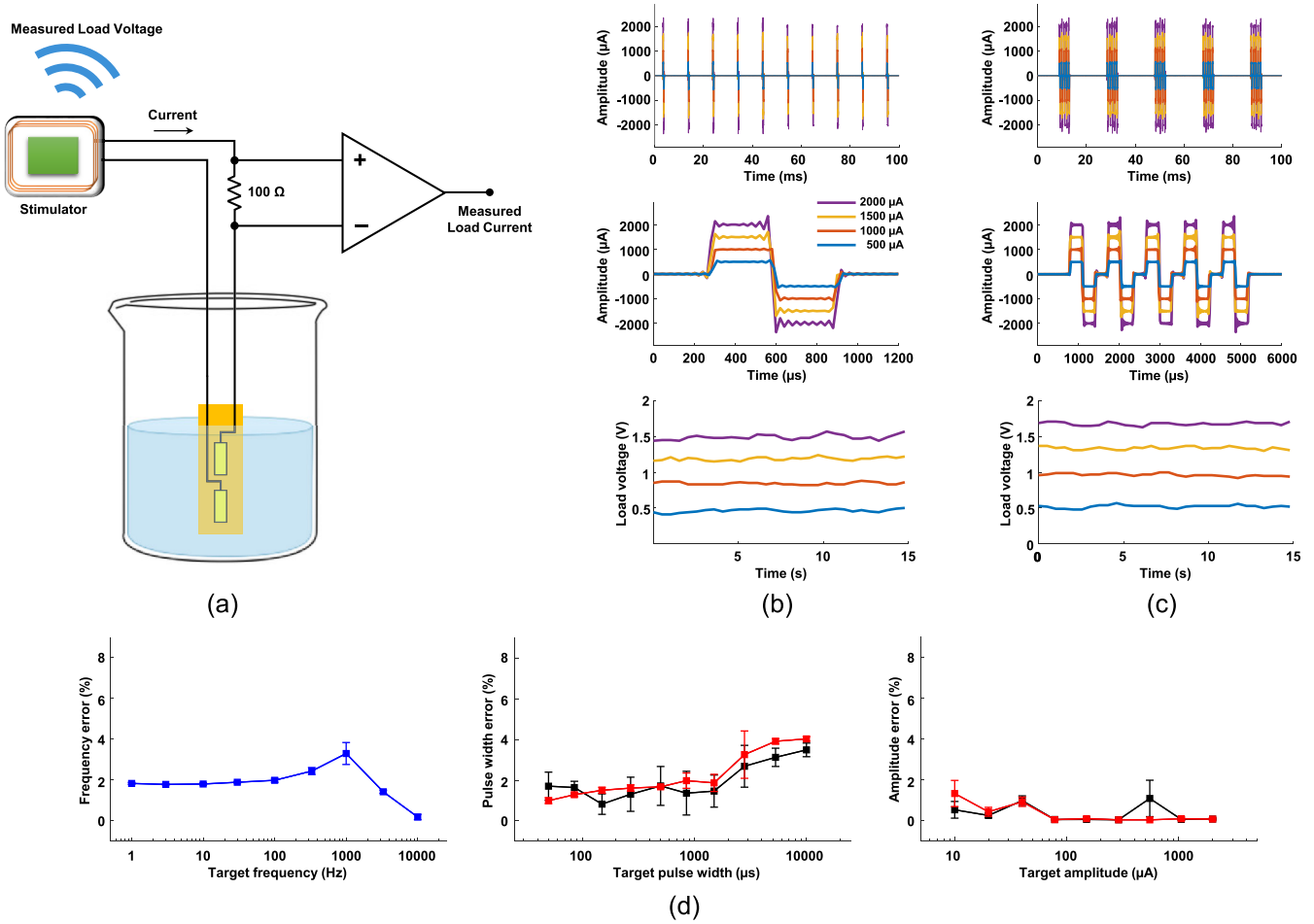

Fig. 10. (a) Experimental setup to evaluate the designed output of the current stimulator, (b) measured load current and voltage with varying stimulation current intensities during conventional stimulation, and (c) burst stimulation. (d) Output error measurements versus input parameters. Red and black lines indicate anodic and cathodic phases, respectively.

inserted epidurally into the dorsal surface of the spinal cord under deep anesthesia. To ensure the accuracy of the electrode location, muscle contraction was measured by increasing the amplitude (4 Hz, 0.2 ms) until both sides of the hindlimb muscles contracted. The electrode was repositioned when each hind limb muscle contracted separately. The electrode was immobilized with sutures using holes on both sides of the electrode body, and the overlying muscles were sutured to cover the electrode. The fascia on the left back was cleared from the space, and the stimulator was implanted into the left side of the back. The rats were allowed to recover for 1 week before the start of stimulation.

To investigate the biocompatibility of the proposed system, the device was implanted into the back of a rat. The anti-inflammatory drug (Metacam, 20 mg/mL solution for injection, Boehringer Ingelheim, Germany) was subcutaneously injected for 3 days. After 3 weeks of implantation, the device was removed for tissue extraction. The surrounding muscle tissue in contact with the implantable device was extracted, immediately immersed in 4% paraformaldehyde (pH 7.4) for 2 days, and then embedded in paraffin. Muscle tissue was crossly sliced into 20 μm-thick sections. The sectioned muscles were dipped in xylene following ethanol series for rehydration and stained with hematoxylin (ab220365, Abcam, UK) and eosin (318906, Sigma-Aldrich, US). Histological analyses of the muscle tissue in both the implanted side (ipsilateral) and non-implanted side (contralateral) were performed at the surface of the muscle.

B. Experimental Protocol

MT was measured in awake rats by increasing the current intensity (4 Hz, 0.2 ms, 10 μA step) until both sides of the hindlimb muscles contracted [27]. To prevent cumulative effect from repeated stimulation sessions during MT measurement, the stimulation current was applied only for very short time under 3 s, and sufficient resting time was provided between each session. Mechanical sensitivity was assessed by paw withdrawal threshold (PWT) using von Frey filaments with a series of eight increasing stiffnesses (0.41–15.10 g, Stoelting, USA) using the up-and-down method [28]. The PWT was evaluated before and after stimulation (pre, immediately, 0.5, 1, 1.5, and 2 h after subthreshold stimulation). Either low- (50 Hz) or high-frequency (1 kHz) stimulation was delivered for 30 min in one session. The stimulation amplitude for PWT measurements was determined by 40 to 80% of MT which was checked for 10 days and the pulse width was fixed

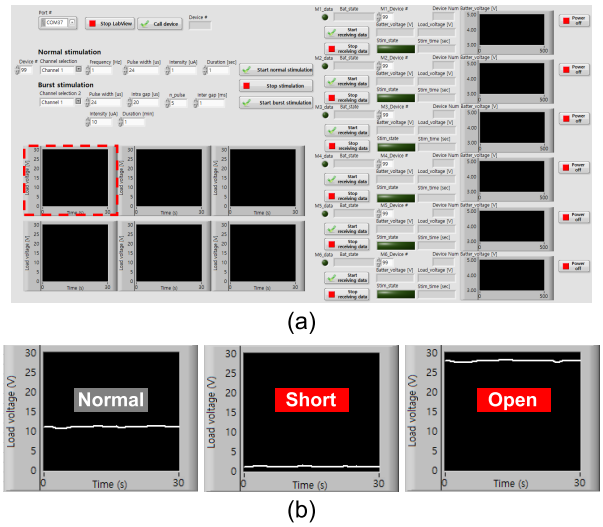

Fig. 11. (a) GUI of the proposed system. Red dotted box indicates the load-monitor. (b) Load-monitoring results with one normal (left) and two defective (middle and right) electrode conditions.

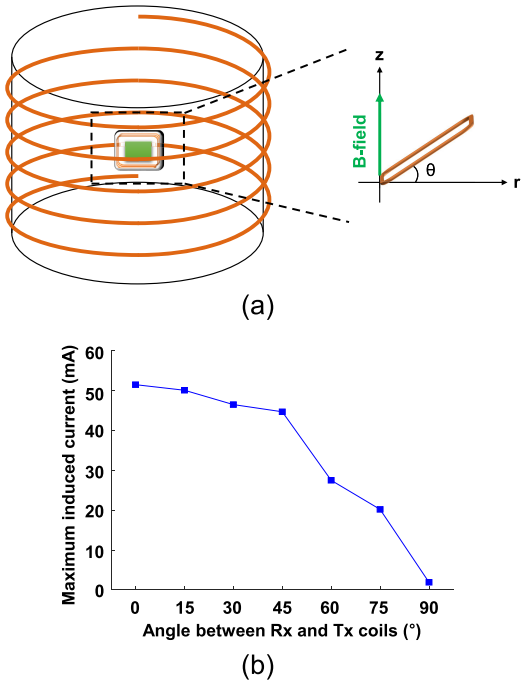

Fig. 12. Wireless charging performance test. (a) Experimental setup of the implantable device and Tx coil. (b) Maximum load current with various tilt angles.

to 0.2 ms in all cases. Only brisk responses involving hind limb withdrawal with complex supraspinal behavior (attention, licking, vocalization, and postural change) were scored.

C. In Vivo Experimental Results

The BBB scores decreased significantly after SCI but increased again over time during the modeling period (Figure 14; Kruskal–Wallis test; $P = 0.0002$; $\chi^2(7) = 28.66$; $n = 4$ animals). After device implantation, the BBB scores showed no significant changes compared with pre-implantation. Rats were able to shift their weight to both

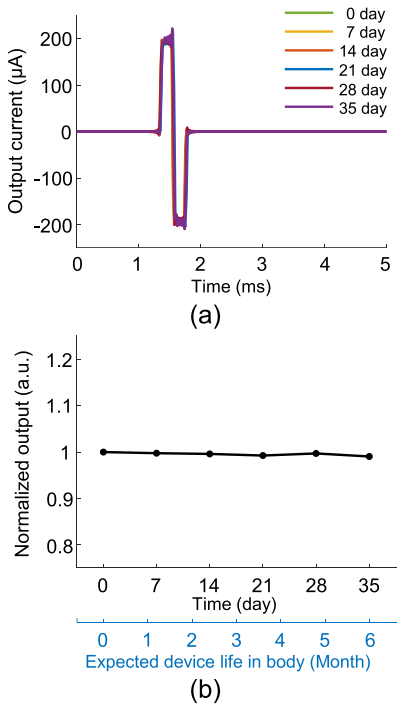

Fig. 13. Accelerated aging test results. (a) Overlapped pulses measured every 7 days for 35 days under accelerated conditions. (b) Output current normalized to current measured at start date.

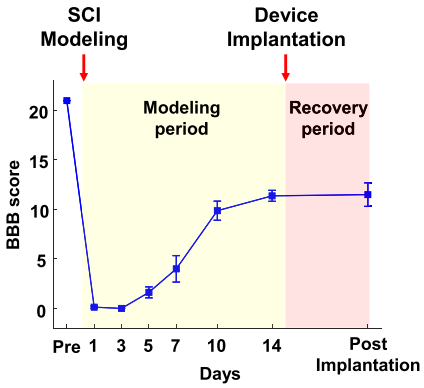

Fig. 14. Investigation of locomotor function in rodents during experiments. The graph depicts data as mean ± SEM.

ipsilateral and contralateral sides. The MTs of the rodent models implanted with the proposed device showed no significant changes over 10 days in the survival experiments (Figure 15; Kruskal–Wallis test; $P = 0.76$; $\chi^2(3) = 1.17$; $n = 4$ animals). In the von Frey test, a significant pain relief effect after stimulation was repeatedly observed in multiple trials over 2 weeks (Figure 16; Kruskal–Wallis test; $P = 0.0055$, 0.2973, and 0.0459 for in-group comparisons, respectively; $n = 4$ animals).

After 3 weeks of device implantation, the skin and fascia were visually assessed before tissue sampling. Skin loosening was observed due to the volume of the implanted device, but the device was located properly under the skin (Figure 17, (a)-(d)). In addition, an inflammation-induced change in fascia was not found in rats. No structural change or

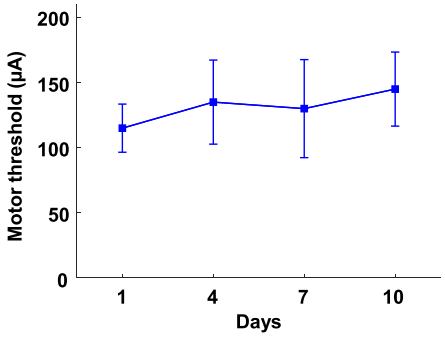

Fig. 15. Changes in motor threshold with stimulation in a spinal cord injury model. The graph depicts data as mean ± SEM.

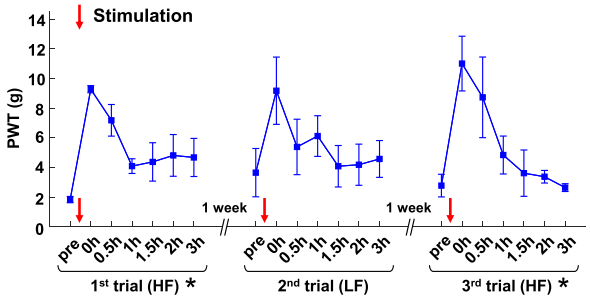

Fig. 16. Pain relief effects after stimulation therapy. The graph depicts data as mean ± SEM. Asterisks denote significant differences, $P < 0.05$.

TABLE IV
BILL OF MATERIALS OF A SINGLE IMPLANTABLE DEVICE

Part	Usage	Manufacturer	Price, USD
4-layer PCB	For mounting components	Seeed	3.99
ATmega328P	Microcontroller	Microchip	5.32
NRF24L01+	2.4GHz RF module	Nordic Semiconductor	1.97
T3168	WPT IC	Taidacent	0.57
TP4056	Battery charger	TPOWER	1.6
AD8684	OP Amp	Analog Devices	7.39
FDC6329L, FDN336P	MOSFET switch	Onsemi	1.2
MAX4535	Analog switch	Maxim Integrated	14.54
MCP4821	DAC	Microchip	3.05
TPS60403	Voltage inverter	Texas Instruments	1.21
TPS61041	Boost Convertor	Texas Instruments	0.78
TPS73233	3.3 V regulator	Texas Instruments	1.41
Other components	Capacitors, inductors, resistors, diodes, pin headers		20
		Total ($)	63.03

tissue damage was found on the muscle surface neighboring the implanted device, but a reduction of tightness of muscles was observed on the ipsilateral side compared to the contralateral side (Figure 17, (e) and (f)). In summary, the *in vivo* results with stimulation during the medium-term experiments and histological findings demonstrated the potential of the proposed implantable device for long-term animal studies.

V. DISCUSSION

In this work, a fully implantable stimulation system was proposed for studying the long-term effect of SCS in SCI

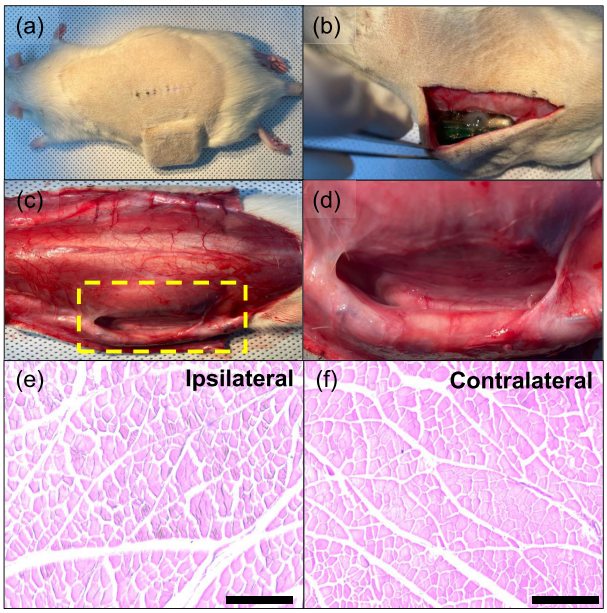

Fig. 17. (a) Photograph of rat implanted with the proposed device. (b) Skin incision to remove the device. (c) Muscle pocket where the device was placed and (d) magnified view. (e, f) Ipsilateral and contralateral histological results, respectively. Scale bars in (e) and (f), 200 μm.

rodent models. The proposed system consists of off-the-shelf components that are relatively inexpensive and easy to get for any researcher. Table IV lists the parts used and their manufacturers, usages, and prices. The total cost of a single implantable device is less than 70 USD, thus we believe this would provide accessibilities and possibilities for simultaneous multi-subject investigations.

To guarantee basic safety and essential performance as an implantable device for preclinical study, the proposed device was designed and validated to meet standards for active implantable medical devices. The device is powered by a 3.7 V Li-Po battery and controlled by 2.4 GHz RF communication, thus electrical isolation from a high-power AC source is fully realized (IEC 60601-1 and ISO 14708-1). In addition, the stimulator provides the biphasic mode to prevent charge buildup during stimulation sessions. With the direct comparisons of pulse width and amplitude during anodic and cathodic phases by following the guidance of ISO 14708-3, it was confirmed that all output errors were within 4% compared with programmed parameters, and there was no significant difference between those two phases in all parametric conditions, demonstrating the device's safety in terms of charge balance issues.

In conventional experimental settings, behavioral and biological investigations of neuropathic pain relief effects are labor-intensive tasks for researchers. Using wireless control and recharging techniques, experimental procedures for MT measurements, von Frey tests, and histological analyses can be simplified, while improving the reproducibility of experiments. Although only 4 rat models were simultaneously handled to determine the potential for the long-term usability of the proposed device in this study, the number of devices that can be controlled at once is limited by the experimental space, not the electrical components. Thus, large-scale experiments

TABLE V
COMPARISON OF RECENT NEUROSTIMULATION SYSTEMS FOR SMALL ANIMAL MODELS

	Paralikar *et al.* [35]	Williams *et al.* [36]	Liu *et al.* [37]	Lee *et al.* [38]	Wright *et al.* [39]	This work
Off-the-shelf	No	No	No	No	Yes	Yes
Lifetime in body	NA	> 3 months	> 7 days	NA	> 5 months	> 6 months
# Stim channels	4	32	16	4	4	4
Stim compliance (V)	NA	10	12	2	12	28
Maximum current (μA)	25000	315	16000	1860	2500	2000
Current resolution (μA)	25	5	0.5 – 2	60	10	10
Timing resolution (μs)	10	NA	10	9	10	1
Stim frequency (Hz)	0.15 – 8.33 k	NA	1.5 – 50 k	13 – 414	0 – 1k	1 – 14.7 k
Load monitoring	No	No	No	No	No	Yes
Wireless telemetry	175 kHz	BLE	BLE	433 MHz	ESB	2.4 GHz
Wireless recharging	100 kHz, < 2.5 cm	Several kHz, < 1 cm	126.7 kHz, < 2 cm	13.56 MHz, Wireless power transfer cage	6.78 MHz, Wireless power transfer cage	175 kHz, Wireless power transfer cage
Dimensions (mm^3)	37.1 × 16.5 × 5.7	13.5 × 12 × 3 + 12.7 × 14 × 3	40 × 20 × 10	30 × 15 × 5	19.9 × 18.1 × 6.6	40.5 × 40.5 × 12.5
Packaging	Titanium	Silicone	Silicone	Epoxy and PDMS	3D-printed shell with coating	Epoxy

with tens or hundreds of animals can be done using the proposed device and one personal computer for wireless control. Furthermore, if the user interface and internet server for remote access will be grafted into the proposed system, the experimental scalability for simultaneous and selective multi-subject experiments would be further expanded [15].

In the von Frey test, temporal changes in PWT after SCS were repeatedly observed in several trials. It has been widely known that the duration of analgesic effect after SCS can continue for hours to days [29], [30]. Similar to previous studies, the pain relief effect observed in this study was sustained for several hours. SCS produces analgesia mediated by spinal gamma-aminobutyric acid (GABA), acetylcholine, serotonin, and opioids [31], [32], [33], [34]. These physiological factors increase after SCS but decrease as time goes on. For this reason, the PWT increased immediately after a stimulation session but decreased over time.

Table V summarizes the key specifications of the proposed device compared to other state-of-the-art works that developed fully implantable devices for small animal studies [35], [36], [37], [38], [39]. Since the proposed device was designed using commercially available electrical and mechanical components, it is relatively inexpensive to manufacture compared to other devices and consequently will be better suited for large-scale experiments. The programmable parameter range of the proposed device is very suitable for SCS investigations using small animals compared to other devices. The superior longevity of the device and wireless charging method using a

WPT cage can accelerate behavioral and biological investigations of SCS and make researchers less labor-intensive.

The proposed device serves as a neurostimulation platform that provides various stimulation parameters with large compliance voltage, high resolution of both stimulation amplitude and frequency, long lifetime via wireless charging, and wireless control function. In addition to SCI, the device can be further utilized to investigate other nervous system disorders in animal models through its versatile functionality. Especially, it can offer significant benefits for many indications requiring long-term evaluation including gastrointestinal disorders [40], bladder dysfunction [41], obesity management [42], and epileptic seizures [43].

While the usefulness of the proposed device was demonstrated via various *in vitro* and *in vivo* approaches, its usability and performance could be further improved with the following works. First, in this study, only one device can be wirelessly charged in the wireless charging cage. Combining the proposed device with simultaneous wireless charging technology for multiple devices [44] can further expand the usefulness of the device. Second, the dimensions of the proposed device were determined based on previous studies performing SCS in rodent models [45]. Further, achieving miniaturization by optimizing components yields more reliable experimental results, as smaller devices are less likely to affect normal motor function or elicit anxiety-related behaviors. Third, in this study, the number of stimulation electrodes was limited to 4 channels, as we intended to confirm only the analgesic effect typically observed after SCS. Embedding multi-channel switches into the proposed device, further precise stimulation would be possible to safely and elaborately control the neuromodulatory effect [43].

VI. CONCLUSION

This paper presents a fully implantable neurostimulation system for long-term behavioral experiments related to neuropathic pain relief research. The system comprised commercially available components, enabling researchers to conveniently implement implantable stimulation systems customized for specific requirements. The operation and performance of the proposed integrated system, including wireless battery charging, bidirectional wireless communication, constant-current stimulation, and therapeutic effects of SCS, were validated via *in vitro* and *in vivo* experiments. As the proposed implantable system was optimized for small animal studies and can be easily customized for various stimulation protocols, we expect that the proposed implantable neurostimulator enables long-term animal experiments for behavioral and biological investigation, paving the way for developing future neuromodulation treatments for neuropathic pain.

REFERENCES

[1] N. Torrance, B. H. Smith, M. I. Bennett, and A. J. Lee, "The epidemiology of chronic pain of predominantly neuropathic origin. Results from a general population survey," *J. Pain*, vol. 7, no. 4, pp. 281–289, Apr. 2006.

[2] J. De Courcy, H. Liedgens, M. Obradovic, T. Holbrook, and R. Jakubanis, "A burden of illness study for neuropathic pain in Europe," *Clinico Econ. Outcomes Res.*, vol. 8, p. 113, Apr. 2016.

[3] R. H. Dworkin et al., "Pharmacologic management of neuropathic pain: Evidence-based recommendations," *Pain*, vol. 132, no. 3, pp. 237–251, 2007.

[4] H. Knotkova et al., "Neuromodulation for chronic pain," *Lancet*, vol. 397, no. 10289, pp. 2111–2124, 2021.

[5] R. Shechter et al., "Conventional and kilohertz-frequency spinal cord stimulation produces intensity- and frequency-dependent inhibition of mechanical hypersensitivity in a rat model of neuropathic pain," *Anesthesiology*, vol. 119, no. 2, pp. 422–432, Aug. 2013.

[6] M. Billot et al., "Comparison of conventional, burst and high-frequency spinal cord stimulation on pain relief in refractory failed back surgery syndrome patients: Study protocol for a prospective randomized double-blinded cross-over trial (MULTIWAVE study)," *Trials*, vol. 21, no. 1, pp. 1–12, Dec. 2020.

[7] Z. Chen et al., "The impact of electrical charge delivery on inhibition of mechanical hypersensitivity in nerve-injured rats by sub-sensory threshold spinal cord stimulation," *Neuromodulation, Technol. Neural Interface*, vol. 22, no. 2, pp. 163–171, Feb. 2019.

[8] J. M. North, K.-S.-J. Hong, and P. Y. Cho, "Clinical outcomes of 1 kHz subperception spinal cord stimulation in implanted patients with failed paresthesia-based stimulation: Results of a prospective randomized controlled trial," *Neuromodulation, Technol. Neural Interface*, vol. 19, no. 7, pp. 731–737, Oct. 2016.

[9] K. P. V. Meuwissen, J. W. Gu, T. C. Zhang, and E. A. J. Joosten, "Burst spinal cord stimulation in peripherally injured chronic neuropathic rats: A delayed effect," *Pain Pract.*, vol. 18, no. 8, pp. 988–996, Nov. 2018.

[10] D. De Ridder, M. Plazier, N. Kamerling, T. Menovsky, and S. Vanneste, "Burst spinal cord stimulation for limb and back pain," *World Neurosurg.*, vol. 80, no. 5, pp. 642.e1–649.e1, Nov. 2013.

[11] J. Paz-Solís, S. Thomson, R. Jain, L. Chen, I. Huertas, and Q. Doan, "Exploration of high- and low-frequency options for subperception spinal cord stimulation using neural dosing parameter relationships: The HALO study," *Neuromodulation, Technol. Neural Interface*, vol. 25, no. 1, pp. 94–102, Jan. 2022.

[12] M. M. Edhi et al., "Time-dynamic pulse modulation of spinal cord stimulation reduces mechanical hypersensitivity and spontaneous pain in rats," *Sci. Rep.*, vol. 10, no. 1, pp. 1–10, Nov. 2020.

[13] B. Harland et al., "A subdural bioelectronic implant to record electrical activity from the spinal cord in freely moving rats," *Adv. Sci.*, vol. 9, no. 20, Jul. 2022, Art. no. 2105913.

[14] M. Nissen, T.-M. Ikäheimo, J. Huttunen, V. Leinonen, and M. von Und Zu Fraunberg, "Long-term outcome of spinal cord stimulation in failed back surgery syndrome: 20 years of experience with 224 consecutive patients," *Neurosurgery*, vol. 84, no. 5, pp. 1011–1018, 2019.

[15] R. Qazi et al., "Scalable and modular wireless-network infrastructure for large-scale behavioural neuroscience," *Nature Biomed. Eng.*, vol. 6, no. 6, pp. 771–786, 2022.

[16] S. M. Won, L. Cai, P. Gutruf, and J. A. Rogers, "Wireless and battery-free technologies for neuroengineering," *Nature Biomed. Eng.*, vol. 7, no. 4, pp. 405–423, 2023.

[17] S. M. Won, E. Song, J. T. Reeder, and J. A. Rogers, "Emerging modalities and implantable technologies for neuromodulation," *Cell*, vol. 181, no. 1, pp. 115–135, Apr. 2020.

[18] B. Chu, "Designing a Li-ion battery charger and load sharing system with microchip's stand-alone Li-ion battery charge management controller," Microchip Technol., Chandler, AZ, USA, Appl. Note AN1149, 2008. [Online]. Available: https://www.microchip.com/en-us/application-notes/an1149

[19] T. Schauer, "Sensing motion and muscle activity for feedback control of functional electrical stimulation: Ten years of experience in Berlin," *Annu. Rev. Control*, vol. 44, pp. 355–374, Jan. 2017.

[20] J. T. Rubinstein, C. A. Miller, H. Mino, and P. J. Abbas, "Analysis of monophasic and biphasic electrical stimulation of nerve," *IEEE Trans. Biomed. Eng.*, vol. 48, no. 10, pp. 1065–1070, Oct. 2001.

[21] B. J. Kim and E. Meng, "Review of polymer MEMS micromachining," *J. Micromech. Microeng.*, vol. 26, no. 1, Jan. 2016, Art. no. 013001.

[22] O. Kim et al., "Spirally arrayed electrode for spatially selective and minimally displacive peripheral nerve interface," *J. Microelectromech. Syst.*, vol. 29, no. 4, pp. 514–521, Aug. 2020.

[23] J. Kim et al., "A wireless power transfer based implantable ECG monitoring device," *Energies*, vol. 13, no. 4, p. 905, Feb. 2020.

[24] D. W. L. Hukins, A. Mahomed, and S. N. Kukureka, "Accelerated aging for testing polymeric biomaterials and medical devices," *Med. Eng. Phys.*, vol. 30, no. 10, pp. 1270–1274, Dec. 2008.

[25] D. M. Basso, M. S. Beattie, and J. C. Bresnahan, "A sensitive and reliable locomotor rating scale for open field testing in rats," *J. Neurotrauma*, vol. 12, no. 1, pp. 1–21, Feb. 1995.

[26] M. W. Carter, K. M. Johnson, J. Y. Lee, C. E. Hulsebosch, and Y. S. Gwak, "Comparison of mechanical allodynia and recovery of locomotion and bladder function by different parameters of low thoracic spinal contusion injury in rats," *Korean J. Pain*, vol. 29, no. 2, pp. 86–95, Apr. 2016.

[27] W. Duan, Q. Huang, F. Yang, S.-Q. He, and Y. Guan, "Spinal cord stimulation attenuates below-level mechanical hypersensitivity in rats after thoracic spinal cord injury," *Neuromodulation, Technol. Neural Interface*, vol. 24, no. 1, pp. 33–42, Jan. 2021.

[28] W. J. Dixon, "Staircase bioassay: The up-and-down method," *Neurosci. Biobehavioral Rev.*, vol. 15, no. 1, pp. 47–50, Mar. 1991.

[29] Y. Maeda, P. W. Wacnik, and K. A. Sluka, "Low frequencies, but not high frequencies of bi-polar spinal cord stimulation reduce cutaneous and muscle hyperalgesia induced by nerve injury," *Pain*, vol. 138, no. 1, pp. 143–152, 2008.

[30] W.-T. Liao, C.-C. Tseng, C.-H. Wu, and C.-R. Lin, "Early high-frequency spinal cord stimulation treatment inhibited the activation of spinal mitogen-activated protein kinases and ameliorated spared nerve injury-induced neuropathic pain in rats," *Neurosci. Lett.*, vol. 721, Mar. 2020, Art. no. 134763.

[31] J.-G. Cui, W. T. O'Connor, U. Ungerstedt, B. Linderoth, and B. A. Meyerson, "Spinal cord stimulation attenuates augmented dorsal horn release of excitatory amino acids in mononeuropathy via a GABAergic mechanism," *Pain*, vol. 73, no. 1, pp. 87–95, Oct. 1997.

[32] Z. Song, C. Ultenius, B. A. Meyerson, and B. Linderoth, "Pain relief by spinal cord stimulation involves serotonergic mechanisms: An experimental study in a rat model of mononeuropathy," *Pain*, vol. 147, no. 1, pp. 241–248, 2009.

[33] Z. Song, B. A. Meyerson, and B. Linderoth, "Spinal 5-HT receptors that contribute to the pain-relieving effects of spinal cord stimulation in a rat model of neuropathy," *Pain*, vol. 152, no. 7, pp. 1666–1673, 2011.

[34] K. L. Sato, E. W. King, L. M. Johanek, and K. A. Sluka, "Spinal cord stimulation reduces hypersensitivity through activation of opioid receptors in a frequency-dependent manner," *Eur. J. Pain*, vol. 17, no. 4, pp. 551–561, Apr. 2013.

[35] K. Paralikar et al., "A fully implantable and rechargeable neurostimulation system for animal research," in *Proc. 7th Int. IEEE/EMBS Conf. Neural Eng. (NER)*, Apr. 2015, pp. 418–421.

[36] I. Williams et al., "SenseBack—An implantable system for bidirectional neural interfacing," *IEEE Trans. Biomed. Circuits Syst.*, vol. 14, no. 5, pp. 1079–1087, Oct. 2020.

[37] F. Liu et al., "A fully implantable opto-electro closed-loop neural interface for motor neuron disease studies," *IEEE Trans. Biomed. Circuits Syst.*, vol. 16, no. 5, pp. 752–765, Oct. 2022.

[38] B. Lee et al., "An implantable peripheral nerve recording and stimulation system for experiments on freely moving animal subjects," *Sci. Rep.*, vol. 8, no. 1, p. 6115, Apr. 2018.

[39] J. P. Wright et al., "A fully implantable wireless bidirectional neuromodulation system for mice," *Biosensors Bioelectron.*, vol. 200, Mar. 2022, Art. no. 113886.

[40] D. T. Berry, J. Choi, C. A. Dexheimer, M. A. Verhaalen, and A. Javan-Khoshkholgh, "An inductively powered implantable system to study the gastrointestinal electrophysiology in freely behaving rodents," *Bioengineering*, vol. 9, no. 10, p. 530, Oct. 2022.

[41] B. Oh et al., "Ultra-soft and highly stretchable tissue-adhesive hydrogel based multifunctional implantable sensor for monitoring of overactive bladder," *Biosensors Bioelectron.*, vol. 225, Apr. 2023, Art. no. 115060.

[42] G. Yao et al., "Effective weight control via an implanted self-powered vagus nerve stimulation device," *Nature Commun.*, vol. 9, no. 1, p. 5349, Dec. 2018.

[43] W. Kang, C. Ju, J. Joo, J. Lee, Y.-M. Shon, and S.-M. Park, "Closed-loop direct control of seizure focus in a rodent model of temporal lobe epilepsy via localized electric fields applied sequentially," *Nature Commun.*, vol. 13, no. 1, p. 7805, Dec. 2022.

[44] J. Yin, D. Lin, C. K. Lee, T. Parisini, and S. Y. Hui, "Front-end monitoring of multiple loads in wireless power transfer systems without wireless communication systems," *IEEE Trans. Power Electron.*, vol. 31, no. 3, pp. 2510–2517, Mar. 2016.

[45] M. van Beek et al., "Long-term spinal cord stimulation alleviates mechanical hypersensitivity and increases peripheral cutaneous blood perfusion in experimental painful diabetic polyneuropathy," *Neuromodulation, Technol. Neural Interface*, vol. 21, no. 5, pp. 472–479, Jul. 2018.